Available online at www.sciencedirect.com
SCIENCE DIRECT®
Solid State Sciences 7 (2005) 1492–1499
Solid State Sciences
www.elsevier.com/locate/ssscie

# Structural and magnetic properties of the solid solution ($0 \leqslant x \leqslant 1$) $YMn_{1-x}(Cu_{3/4}Mo_{1/4})_xO_3$

Sylvie Malo [a,*], Antoine Maignan [a], Sylvain Marinel [a], Maryvonne Hervieu [a], Kenneth R. Poeppelmeier [b], Bernard Raveau [a]

[a] *Laboratoire CRISMAT, UMR CNRS ENSICAEN 6508, 6 bd Maréchal Juin, 14050 Caen Cedex 4, France*
[b] *Department of Chemistry, Northwestern University, 2145 Sheridan Road, Evanston, IL 60208-3113, USA*

Received 14 June 2005; accepted 27 July 2005

Available online 25 October 2005

**Abstract**

Recently, the ferroelectromagnet $YMnO_3$ has been the focus of interest because it exhibits both antiferromagnetism (Néel temperature ~ 80 K) and ferroelectricity (Curie temperature ~ 914 K). There have been no reports of complete $YMn_{1-x}M_xO_3$ solid solutions in which substitution of the foreign $M$ cation preserves the hexagonal $P6_3cm$ structure. In contrast there exist several homeotypic phases with the general formula, $Ln_{1+n}Cu_nMO_{3+3n}$ ($n = 1$ ($M$ = Ti), 2 ($M$ = V) and 3 ($M$ = Mo); *Ln*: lanthanide). Several $YMn_{1-x}(Cu_{3/4}Mo_{1/4})_xO_3$ compounds have been synthesized. The solid solution, from $YMnO_3$ ($x = 0$) to $YCu_{3/4}Mo_{1/4}O_3$ ($x = 1$) has been characterized by X-ray diffraction and transmission electron microscopy study. For $0 < x < 0.9$, the compounds are found to crystallize in the non-centrosymmetric structure, space group $P6_3cm$, of $YMnO_3$. The Mn-free end member, $x = 1$, crystallizes in a complex multiple cell, the superstructure being associated to $Cu^{3+}/Mo^{6+}$ cationic ordering. Dilution of the $Mn^{3+}$ magnetic array by the paramagnetic ($Cu^{2+}$) and diamagnetic ($Mo^{6+}$) cations is found to decrease the antiferromagnetic ordering temperature and it becomes undetectable for $x \geqslant 0.5$ compositions.


*Keywords:* Hexagonal structure; Electron Microscopy; Solid solution; Magnetic properties

## 1. Introduction

Among the fascinating properties of the perovskite manganites, the ferroelectricity of the hexagonal phase "type $YAlO_3$" has been revisited after the new interest of the solid state scientists for the search of new multiferroïc materials (see Ref. [1] and references therein), which are promising materials for applications in the information storage spintronics and sensor. Those properties result from the strong interplay between spin, charge and orbital ordering, responsible for simultaneous ferromagnetism, ferroelectricity and ferroelasticity. The $YMnO_3$ hexagonal phase is a typical example of a magnetic ferroelectric with a magnetic Néel temperature $T_N \sim 80$ K and a ferroelectric Curie temperature $T_C \sim 914$ K [2–5]. For this phase a clear anomaly in the dielectric constant at $T_N$ has been found [5].

From the structural point of view, the $RMnO_3$ hexagonal structure differs strongly from the ideal cubic and distorted orthorhombic perovskite and is generally stabilized for small enough $R$ cation in $RMnO_3$ ($R$ are lanthanides smaller than $Tb^{3+}$, $Sc^{3+}$ and $Y^{3+}$) [2,6,7]. The Mn cations adopt a fivefold trigonal bipyramidal coordination contrasting with its octahedral coordination in the "classical" perovskite. Accordingly, the framework of the hexagonal phase (space group $P6_3cm$) is built from the stacking along the $c$-axis of layers built of corner sharing ($MnO_5$) trigonal bipyramids (Fig. 1). This coordination of Mn leads to a crystal field splitting, different from the octahedral one, with an unoccupied $d_{z^2}$ orbital hybridized with the $p_z$ orbital of oxygen along the $c$-direction. This has been previously proposed to be at the origin of a "one-dimensional $d^0$-ness" which is original compared to usual "$d^0$-ness criterion" for ferroelectricity [8].

There exist only a few reports describing substitutions at the Mn-site in $YMnO_3$, which preserve the hexagonal structure. As for the substitution of cobalt for manganese in $YMnO_3$, though

* Corresponding author. Tel.: +33 2 31 45 26 10.
*E-mail address:* sylvie.malo@ensicaen.fr (S. Malo).

1293-2558/$ – see front matter 
doi:10.1016/j.solidstatesciences.2005.07.003

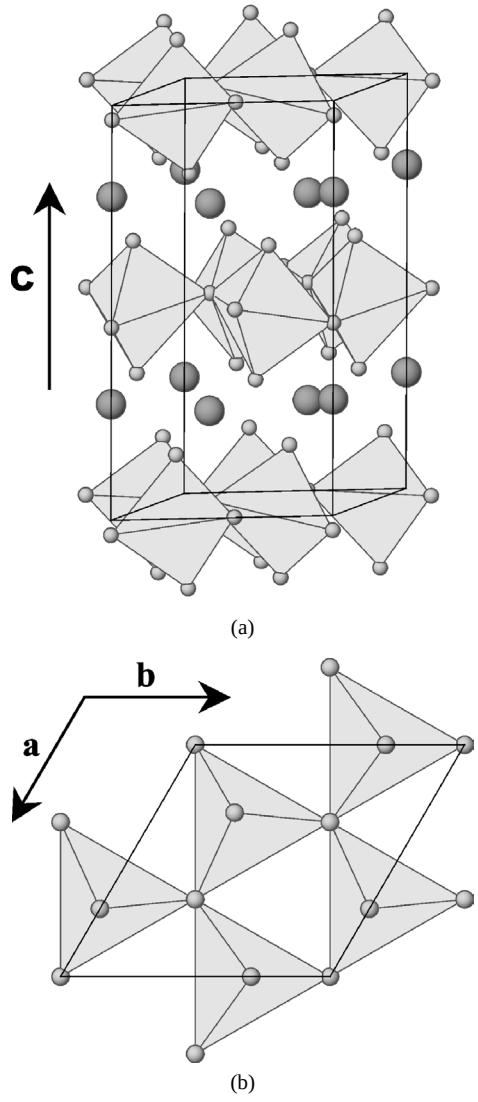


Fig. 1. (a) The structure of $YMnO_3$, an example of the $P6_3cm$ hexagonal structure type and (b) (001) projection of the $MnO_5$ trigonal bipyramids plane in $YMnO_3$.

the solubility range is important, the structure transforms to an orthorhombic one as soon as $x = 0.15$ in $YMn_{1-x}Co_xO_3$ [9]. In this respect, $LaCu_{3/4}Mo_{1/4}O_3$ is a very interesting phase since, despite the large ionic radius of $La^{3+}$, it also crystallizes in the hexagonal structure [10,11]. This provides a nice illustration of the unpredictability in solid-state chemistry. The "improbable" formation of many oxides has been explained on the basis of a balance between stable and unstable compositions [12]. In fact, there exists a large family of closely related oxides containing copper, that crystallize in hexagonal structures. Their chemical formula can be written $Ln_{1+n}Cu_nMO_{3+3n}$ where $Ln$ and $M$ are lanthanide and a $d^0$ cation, respectively. The three first members of this series ($n = 1$, 2 and 3) are represented by the compounds $A_2CuTiO_6$ ($A$ = Y, Tb–Lu) [13], $La_3Cu_2VO_9$ [14,15] and $A_4Cu_3MoO_{12}$ ($A$ = La–Nd, Sm–Lu) [10–12] respectively. These different $Cu^{2+}$ containing phases can be further classified into two categories: random occupation of the trigonal pyramids by the cations (Cu : Ti ratio is 1 : 1) for the $n = 1$ member leading to the same $P6_3cm$ space group as $YMnO_3$, whereas the 2 : 1 ratio of Cu : V and the 3 : 1 ratio of Cu : Mo for the $n = 2$ and $n = 3$ members lead to supercells related to cation ordering on the triangular network of cations (see Table 1). These cation ordering patterns lead to original magnetic properties as for the $La_4Cu_3MoO_{12}$ ordered hexagonal structure in which the geometric frustration of the $Cu^{2+}$–O–$Cu^{2+}$ antiferromagnetic interactions are at the origin of a magnetic behavior much like that of the Kagomé lattice [16,17]. Taking into consideration this series of hexagonal compounds, we studied the possible solid solution between $YMnO_3$ and the $n = 3$ member of the series $La_4Cu_3MoO_{12}$.

In the present paper, we report on the structural and magnetic properties of several compounds within the system $YMn_{1-x}(Cu_{3/4}Mo_{1/4})_xO_3$ for $0 \leqslant x \leqslant 1$. These compositions, for $0 \leqslant x < 0.9$, are single-phase and exhibit the hexagonal "$YAlO_3$-type" structure whereas for the end member corresponding to $x = 1$, a superstructure due to the Cu/Mo cationic ordering is found. The samples with intermediate manganese content ($0.9 \leqslant x < 1$) present the hexagonal subcell characteristic of $YAlO_3$ and additional reflections involving a supercell derived from the $x = 1$ structure. The $(Cu_{3/4}Mo_{1/4})^{3+}$ substitution for $Mn^{3+}$ is found to progressively decrease the $Mn^{3+}$–$Mn^{3+}$ antiferromagnetic interactions. For the end member, $YCu_{3/4}Mo_{1/4}O_3$, the cationic ordering is responsible for the very low effective paramagnetic moment observed.

## 2. Experimental

Polycrystalline samples of $YMn_{1-x}(Cu_{3/4}Mo_{1/4})_xO_3$ ($0 \leqslant x \leqslant 1$ with $x = 0$; 0.25; 0.5; 0.75; 0.85; 0.9; 0.95 and 1) were synthesized at ambient pressure by solid-state reaction of stoichiometric amounts of $Y_2O_3$, $Mn_2O_3$, CuO and $MoO_3$. Powders were ground in an agate mortar, pressed in bars ($\sim 2$ mm $\times$ 2 mm $\times$ 10 mm) and heated to 1100 °C at a rate of 1.5 °C/min, held at this temperature for 24 hours and cooled to room temperature at a rate of 70 °C/h.

The electron diffraction (ED) study was carried out on a JEOL 200CX electron microscope fitted with an eucentric goniometer (±60°) equipped with an EDS analyzer. For the transmission electron microscopy study, the samples were crushed in alcohol and deposited on a holey carbon membrane supported by a nickel grid.

The powder X-ray diffraction (PXRD) data were recorded using a Philips vertical diffractometer, working with Cu K$\alpha$ radiation in the range $10 \leqslant 2\theta \leqslant 100°$ with a step size of 0.02°.

The magnetic properties have been studied by using a SQUID magnetometer. The sample under study was first cooled in the absence of magnetic field down to 5 K, temperature at which a magnetic field of 0.3 T was applied. The magnetic moment values were then collected as a function of temperature between 5 and 400 K. Additional isothermal magnetic field dependent magnetization curves were collected at 5 K.

Table 1
Comparative data of the derivatives of $YAlO_3$ type structures

| Composition | N.O. B, B′ site | Sym. /Ref. | Lattice parameters | $Z$ | $r_B$ (Å) | $r_A/r_B$ | Ratio $B^{5+,6+}/\sum(B)$ |
|---|---|---|---|---|---|---|---|
| $YAlO_3$ | III | Hex.<br>Type I<br>[4,18] | $a \approx 3.68$ Å<br>$c \approx 10.521$ Å | 1 | 0.48 | 2.12 | – |
| $InMnO_3$[a] | III | Hex.<br>Type II<br>[21] | $a \approx 3.33$ Å<br>$c \approx 12.18$ Å | 1 | 0.58 | 1.59[a] | – |
| $YMnO_3$ | III | Hex.<br>[2] | $a \approx 6.14$ Å<br>$c \approx 11.41$ Å | 3 | 0.58 | 1.76 | 0 |
| $YMn_{0.15}Cu_{0.64}Mo_{0.21}O_3$ | III/II/VI | Hex.<br>This article | $a \approx 6.263$ Å<br>$c \approx 11.323$ Å | 3 | 0.607 | 1.68 | 0.21 |
| $YCu_{0.5}Ti_{0.5}O_3$ | II/IV | Hex.<br>[13] | $a \approx 6.17$ Å<br>$c \approx 11.48$ Å | 3 | 0.59 | 1.72 | – |
| $YCu_{0.75}Mo_{0.25}O_3$ | II/VI | Monocl.<br>This article | $a \approx 7.2$ Å<br>$b \approx 6.2$ Å<br>$c \approx 11.8$ Å<br>$\beta \approx 107°$ | 4 | 0.61 | 1.66 | 0.25 |
| $LaCu_{0.75}Mo_{0.25}O_3$ | II/VI | Monocl.<br>[16] | $a \approx 7.9$ Å<br>$b \approx 6.9$ Å<br>$c \approx 11$ Å<br>$\gamma \approx 90°$ | 4 | 0.61 | 1.90 | 0.25 |
| $LaCu_{2/3}V_{1/3}O_3$ | II/V | Hex.<br>[12] | $a \approx 14.4$ Å<br>$c \approx 10.7$ Å | 13 | 0.587 | 1.97 | 0.33 |

[a] Calculated for eightfold coordination of $In^{3+}$, but in the $InMnO_3$, the $In^{3+}$ coordination is octahedral.

## 3. Structural results

### 3.1. Powder X-ray diffraction

The powder X-ray diffraction data, collected at room temperature on the samples $YMn_{1-x}(Cu_{3/4}Mo_{1/4})_xO_3$ with $x = 0$; 0.25; 0.5; 0.75; 0.85; 0.9; 0.95 and 1, give evidence to the good crystallinity of the samples. Regardless of the $x$ value, the PXRD patterns were similar to that of the undoped hexagonal $YMnO_3$ phase [2], which indicates that they crystallized in the same type of structure (Fig. 2). Despite this similarity, one can observe the variation of the relative intensity of some peaks, indexed in the hexagonal cell, with the manganese content as, for example, the intensity decrease of the (102) peak ($2\theta \approx 23°$) with $x$. $YMnO_3$ crystallizes at room temperature in an hexagonal cell with $a \approx 6.14$ Å and $c \approx 11.41$ Å and a $P6_3cm$ symmetry characterized by the conditions limiting the reflections $h0\bar{h}l$: $l = 2n$. The structure can be described as a stacking along $c$ of layers of $MnO_5$ trigonal bipyramids (Fig. 1(a)), corner sharing of the trigonal basal plane O atoms (Fig. 1(b)) and forming cages where are located the Y-cations in an eightfold coordination.

The lattice parameters and calculated volumes obtained from the PXRD data are listed in Table 2. It clearly appears (Fig. 3) that the $a$ parameter increase with $x$, whereas $c$ decreases and, more important, that the evolution of the cell parameters versus $x$ follows the Vegard law up to $x = 0.85$. In this part of the diagram, the volume of the hexagonal cell increases in agreement with the increase of the average size of the B-cation ($\langle r_{Cu^{2+}_{3/4}Mo^{6+}_{1/4}} \rangle \sim 0.61$ Å, $r_{Mn^{3+}} \sim 0.58$ Å). This monotonous evolution of the parameters suggests a random distribution of the three types of cations on the B-sites.

Table 2
Lattice parameters obtained from PXRD refinement of $YMn_x(Cu_{3/4}Mo_{1/4})_xO_3$

| $x$ | $a$ (Å) | $c$ (Å) | $V$ (Å$^3$) |
|---|---|---|---|
| 0 | 6.1453(2) | 11.3714(5) | 371.90391 |
| 0.25 | 6.1831(1) | 11.3665(3) | 376.33094 |
| 0.5 | 6.2176(2) | 11.3521(6) | 380.0602 |
| 0.75 | 6.2483(1) | 11.3407(3) | 383.4372 |
| 0.85 | 6.2623(1) | 11.329(3) | 384.7600 |
| 0.9 | 6.2629(1) | 11.3228(3) | 384.6231 |
| 0.95 | 6.2668(2) | 11.3131(4) | 384.7724 |
| 1 | 6.2645(3) | 11.3091(7) | 384.35409 |

For $x \geqslant 0.9$, one observes a variation of the parameters evolution: the $a$ parameter remains roughly constant whereas $c$ abnormally decreases. The volume remains constant despite the increase of the average $r_B$ size, suggesting a rearrangement of the B-cations. This hypothesis is reinforced by the presence of small extra reflections on the PXRD patterns (Fig. 3).

### 3.2. Electron diffraction study

#### 3.2.1. The $YMnO_3$-type solid solution $0 \leqslant x < 0.9$

The electron diffraction characterization was carried out for all the samples with $x < 0.9$ at room temperature. The reciprocal space was reconstructed by tilting around the $c^*$ and

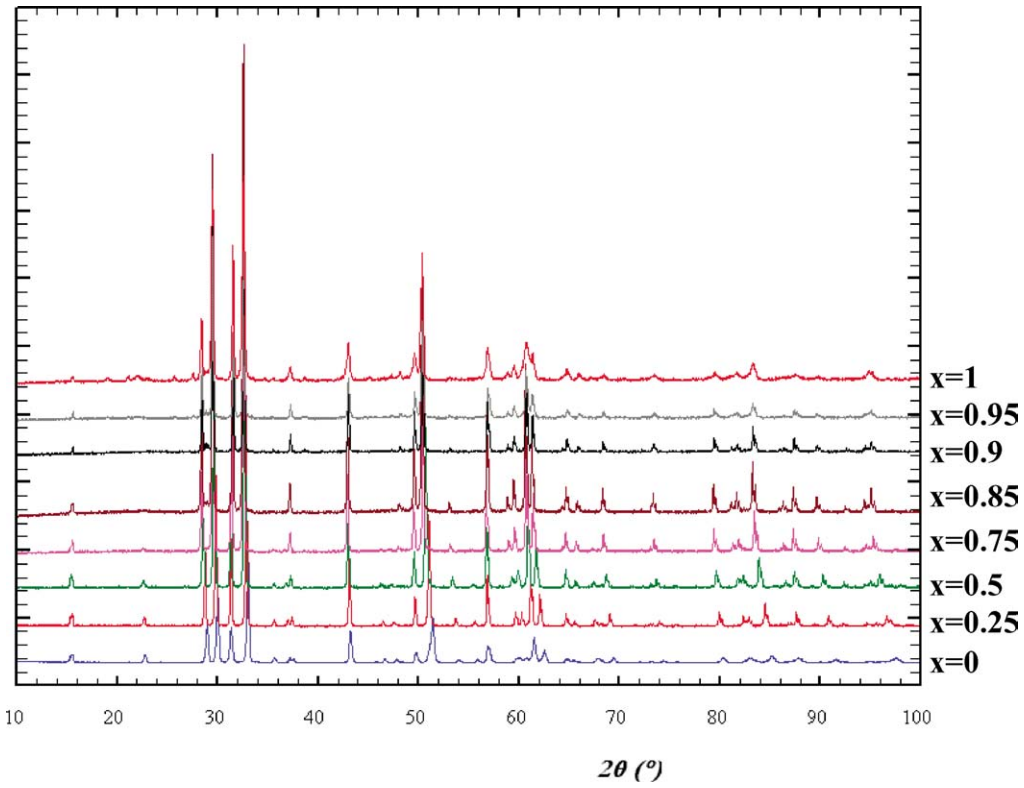


Fig. 2. Powder X-ray diffraction data for $YMn_{1-x}(Cu_{3/4}Mo_{1/4})_xO_3$ ($0 \leqslant x \leqslant 1$).

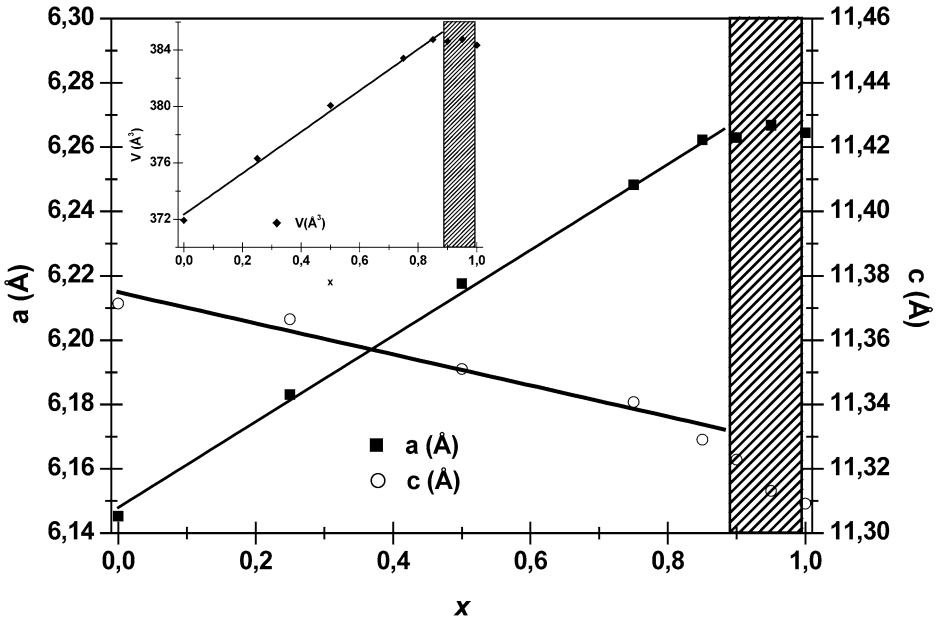


Fig. 3. Evolution of the lattice parameters and volume versus $x$ in $YMn_{1-x}(Cu_{3/4}Mo_{1/4})_xO_3$.

$a^*$ axes. They confirm that the cell parameters, $a \approx 6.2$ Å and $c \approx 11.35$ Å, and the conditions of reflection of the $P6_3cm$ space group ($h0\bar{h}l$: $l = 2n$) are in agreement with those of the undoped $YMnO_3$ phase [2]. The ED patterns of $YMn_{0.5}(Cu_{3/4}Mo_{1/4})_{0.5}O_3$ recorded along [0001]; [11$\bar{2}$0] and [10$\bar{1}$0] are given as example in Fig. 4. For all the samples of the solid solution ($0 \leqslant x \leqslant 0.85$) one observes extra extinction with regard to the $P6_3cm$ space group. The reflections indexed $h0\bar{h}0$ with $h \neq 3n$, are indeed systematically extinguished in the [0001] ED pattern (Fig. 4(a)) and barely visible in the [11$\bar{2}$0] ED pattern (Fig. 4(b)) owing to double diffraction phenomena. The extra extinction of the $h0\bar{h}0$ diffraction spots results from the particular atomic position ($x$ 0 0 with $x \approx 1/3$) of the B-cation. Considering only the (001) plane of the $YMnO_3$

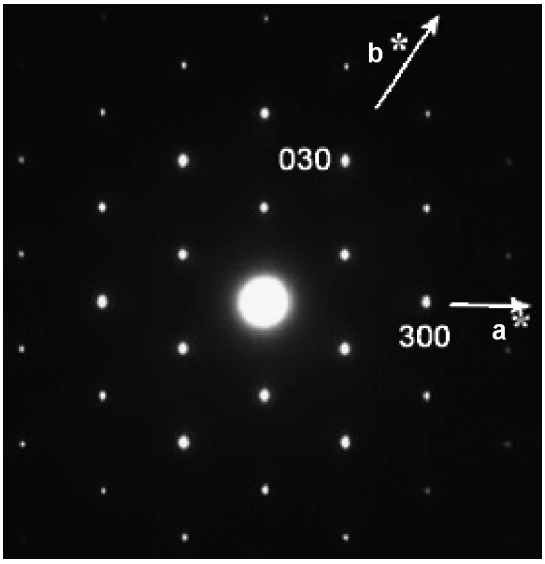


(a)

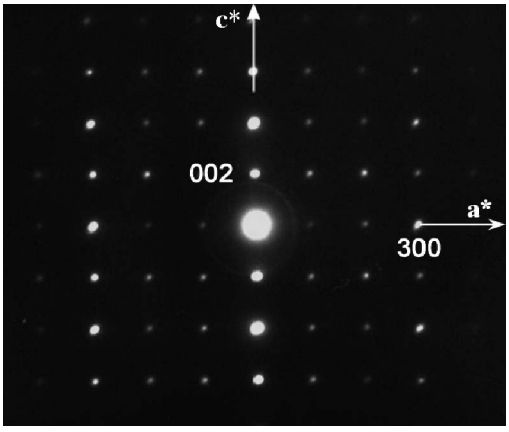


(b)

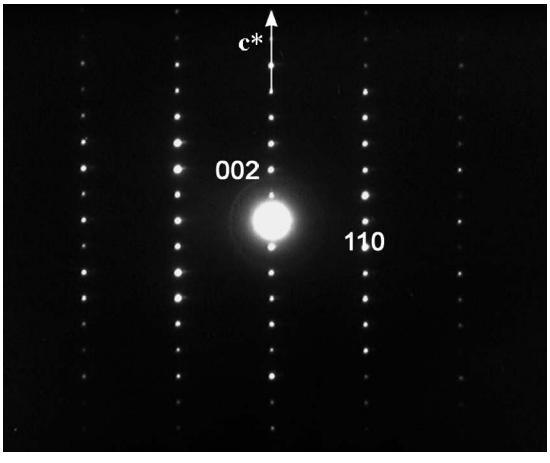


(c)

Fig. 4. ED patterns of $YMn_{1-x}(Cu_{3/4}Mo_{1/4})_xO_3$ ($x = 0.5$) recorded along the (a) [0001], (b) [11$\bar{2}$0] and (c) [10$\bar{1}$0] zone axis.

phase (Fig. 5), the projected structure could be described by a smaller cell when the Mn is located in a crystallographic site very close to 1/3 0 0. This smaller cell, represented by the dashed line on Fig. 5, corresponds to the hexagonal cell ($a \approx 3.68$ Å and $c \approx 10.52$ Å) characterizing $YAlO_3$ [18], that

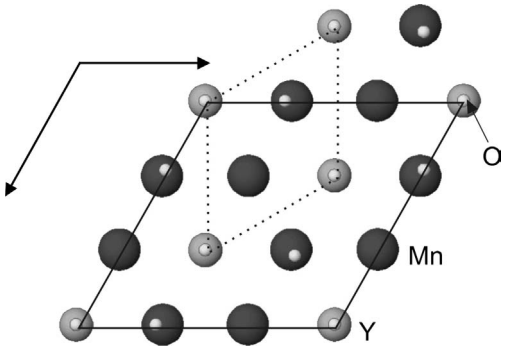


Fig. 5. (001) projection of the hexagonal $YMnO_3$ structure. The dashed lines represent the $YAlO_3$-type hexagonal cell.

is 3 times smaller (see Table 1). The experimental (0001)* ED pattern (Fig. 4(a)) recorded for $YMn_{0.5}(Cu_{3/4}Mo_{1/4})_{0.5}O_{3-\delta}$ appears therefore similar to the (0001)* ED pattern calculated for $YAlO_3$ ($Z = 1$) and to the (0001)* ED pattern calculated for $YMnO_3$ ($Z = 3$) with Mn located in (1/3 0 0). Considering the whole structure, the tilting of the $MnO_5$ polyhedra and the waving of the "[YO]" layer imply to use a triple cell ($Z = 3$) and a lower symmetry ($P6_3cm$ instead of $P6_3/mmc$) for describing the hexagonal $YMnO_3$ structure.

The important point highlighted by the ED study of $YMn_{1-x}(Cu_{3/4}Mo_{1/4})_xO_3$ is that the $(Cu_{3/4}Mo_{1/4})^{3+}$ substitution for $Mn^{3+}$ allows stabilizing the sample whatever $x$ ($0 \leqslant x \leqslant 0.85$) preserves the $YMnO_3$-type hexagonal structure. Accounting that there is only one site for the B-cation in the $P6_3cm$ structure, it means that $Mn^{3+}$, $Cu^{2+}$ and $Mo^{6+}$ are randomly distributed over a single site up to $x < 0.9$. Moreover, the extinction of the $h0\bar{h}0$ with $h \neq 3n$ reflections in the ED patterns recorded on the samples $0 \leqslant x \leqslant 0.85$ points out that these cations occupy similar $x$ 0 0 with $x \sim 1/3$ positions. The simulated electron diffraction patterns, calculated with the $P6_3cm$ structure changing only slightly the $x$ value of the B-site, showed indeed the great sensitivity of the intensity of the $h0\bar{h}0$ reflections for tiny deviation with regard to the $x = 1/3$ peculiar position.

### 3.2.2. *A new type of ordering for $x = 1$*

For $YCu_{3/4}Mo_{1/4}O_3$ ($x = 1$), the ED patterns recorded on the manganese-free sample present extra reflections in addition to the reflections typical of the basic ($Z = 1$) $YAlO_3$-type structure. On the ED pattern recorded along [010], extra reflections are observed with regard to the hexagonal subcell, which imply to define a monoclinic cell with $\vec{a}^*_m = \frac{3}{4}\vec{a}^*_h + \frac{1}{2}\vec{c}^*_h$; $\vec{b}^*_m = \frac{\vec{a}^*_h + \vec{b}^*_h}{2}$ and $\vec{c}^*_m = \vec{c}^*_h$, where the subscripts m and h designate the monoclinic and the simple hexagonal cells respectively. This monoclinic cell is then characterized by a $\approx 7.2$ Å, $b \approx 6.2$ Å, $c \approx 11.8$ Å and $\beta \approx 107°$ with the following conditions limiting the reflections: $h0l$: $l = 2n$, compatible with the space groups P c, P 2/c or P $2_1$/c. The ED patterns of the basis planes are given in Fig. 6. Most of the crystallites studied by electron diffraction present twinned domains. The additional spots which result from this twinning are indicated by white arrows on the (010)* ED pattern (Fig. 6(a)).

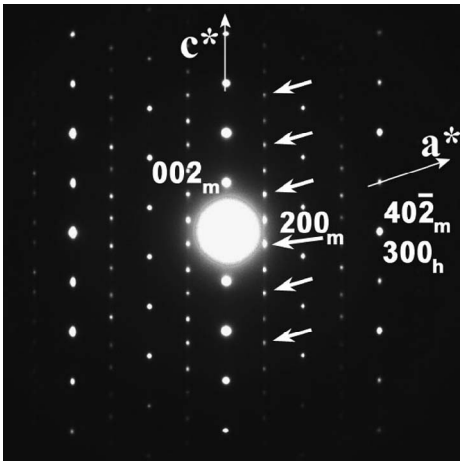


(a)

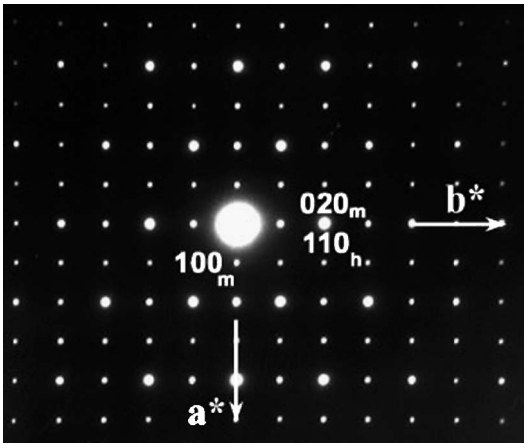


(b)

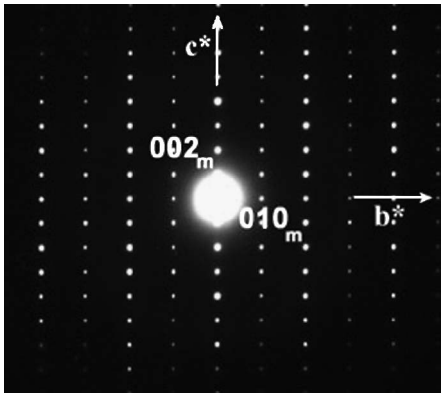


(c)

Fig. 6. ED patterns of $YCu_{3/4}Mo_{1/4}O_3$ recorded along (a) [010], (b) [$\bar{1}$04] and (c) [40$\bar{1}$]. The white arrows on the (010)* ED pattern indicate the extra spots due to twinned domains. The subscript h refers to the hexagonal unit cell while the subscript m refers to the monoclinic supercell.

### 3.2.3. *Multiphased domain for* $0.9 \leqslant x < 1$

For this part of the diagram, some ED patterns exhibiting diffuse extra reflections, which are characteristic of $x = 1$ ordering, have been detected. However, these extra reflections are not systematically observed for all the crystallites and, even, different domains can be observed. The EDS analyses of these crystallites and domains do not exhibit significant deviation of the cationic ratio. One can conclude, that according to our conditions of synthesis, the $0.9 \leqslant x < 1$ domain is multiphased and symbolized by a grey rectangle in Fig. 3.

Table 3
Atomic parameters for selected $YMn_{1-x}(Cu_{3/4}Mo_{1/4})_xO_3$ from XRPD refinements

| $x$ | 0 | 0.25 | 0.5 | 0.75 |
|---|---|---|---|---|
| Y(1) $z$ | 0.280(2) | 0.273(2) | 0.281(2) | 0.278(2) |
| Y(2) $z$ | 0.238(2) | 0.237(2) | 0.252(2) | 0.255(1) |
| Mn $x$ | 0.338(4) | 0.330(3) | 0.332(4) | 0.332(3) |
| O(1) $x$ | 0.293(4) | 0.308(5) | 0.302(8) | 0.308(5) |
| O(1) $z$ | 0.155(2) | 0.161(2) | 0.164(4) | 0.155(3) |
| O(2) $x$ | 0.651(4) | 0.644(5) | 0.660(9) | 0.658(7) |
| O(2) $z$ | 0.332(2) | 0.346(2) | 0.336(4) | 0.339(3) |
| O(3) $z$ | 0.464(5) | 0.492(3) | 0.506(5) | 0.517(4) |
| O(4) $z$ | 0.015(4) | 0.024(2) | 0.040(4) | 0.041(2) |
| $R_{Bragg}$ (%) | 7.65 | 8.47 | 8.60 | 12 |

The space group is $P6_3cm$. Atomic positions: Y(1) at 2*a* (0, 0, *z*), Y(2) at 4*b* (1/3, 2/3, *z*), Mn; Cu and Mo randomly distributed at 6*c* (*x*, 0, 0), O(1) and O(2) at 6*c* (*x*, 0, *z*), O(3) at 2*a* (0, 0, *z*) and O(4) at 4*b* (1/3, 2/3, *z*).

### 3.3. *Structural remarks*

On the basis of the electron diffraction study, structure refinements have been carried out for the solid solution $0 \leqslant x < 0.9$, using the powder X-ray diffraction data. The atomic parameters and reliability factors are given in Table 3. They are in agreement with the hypothesis of a random positions of the cations located in the B-site, namely $Mn^{3+}$, $Cu^{2+}$ and $Mo^{6+}$.

The monoclinic supercell of the $YCu_{3/4}Mo_{1/4}O_3$ ($x = 1$), has never been reported, at our knowledge. The *c* parameters of numerous derivative structures, ordered or non-ordered, are of the same order as that of $YAlO_3$, ranging from 10.5 to 11.5 Å. The usual factors commonly explored for understanding the differences in the cell parameters and symmetry of structural families are compared in Table 1, namely the mismatch of the cationic radius between the A- and the B-sites, size mismatch on the B-site and the oxidation state of the cations:

- The role of the mismatch of the cationic radius between the A- and the B-sites appears crucial for $A^{3+}B^{3+}O_3$, as shown by comparing $YAlO_3$, $YMnO_3$ and $InMnO_3$. Decreasing $r_A/r_B$ by increasing $r_B$, from 2.12 $YAlO_3$ ($Z = 1$, SG = $P6_3$/mmc) to 1.76 for $YMnO_3$ induces a distorted triple cell ($Z = 3$, SG = $P6_3cm$) keeping the eightfold coordination of Y. In a different way, decreasing $r_A/r_B$ from 1.76 by decreasing $r_A$ from $YMnO_3$ ($Z = 3$, SG = $P6_3cm$) to 1.59 for $InMnO_3$ leads to a simple cell ($Z = 1$, SG = $P6_3$/mmc), which how differ from that of $YAlO_3$ since the mismatch is accommodated by a smaller distance of next-nearest neighbor O anions, indium being in six fold coordination (and significant decrease of **a** and increase of **c**).
- The balance by introducing two cations in the B-site, $A^{3+}(B,B')^{3+}O_3$ properly selected to respect the $r_A/r_B$ criterium. For example, as reported by Floros et al. [13] the sample $Y_2CuTiO_6$ ($r_A/r_B = 1.72$ see Table 1) maintains hexagonal symmetry of the triple cell $YMnO_3$ ($Z = 3$,

SG = P6$_3$cm) with no cationic ordering as in the title solid solution with three cations randomly distributed at the B-site, $YMn_{1-x}(Cu_{3/4}Mo_{1/4})_xO_3$ for $x < 0.9$.
- $YCu_{3/4}Mo_{1/4}O_3$ and $LaCu_{3/4}Mo_{1/4}O_3$, which exhibit the same (BB′) cations (by the way, same $r_B$) but strongly different $r_A/r_B$ (1.66 and 1.93, respectively), are both ordered. They both involve a quadrupling of the subcell, but the ordering mode are different as well in the (001) planes as in their stacking along [001].

On the basis of these remarks, it appears that, on the one hand, the distortion-type strongly depends on $r_A/r_B$ and that, on the other hand, long range ordering is clearly generated by the presence, on the B-site, of two cations exhibiting very different oxidation states, a very high $B'^{5+}$ or $B'^{6+}$ and a lower one $B^{2+}$. This mechanism is exactly the same as the one observed in the ordered perovskite. In both cases, the ratio between the two types of cations, $B'^{5+,6+}/(B'^{5+,6+} + B^{2+})$ is a critical parameter.

## 4. Magnetic properties

The $T$ dependent inverse magnetic susceptibility ($\chi^{-1}$) measurements of $YMn_{1-x}(Cu_{3/4}Mo_{1/4})_xO_3$ samples are illustrated by the curves given in Fig. 7. For all compositions, the $\chi^{-1}(T)$ curve can be fitted by a Curie–Weiss law of the type $\chi = \frac{C}{T-\theta_p}$ in the higher $T$ region as shown by the straight lines in Fig. 7. The corresponding $\theta_p$ and effective paramagnetic moment $\mu_{eff}$ values are reported in Table 4. As shown in the table, $|\theta_p|$ decreases as $x$ increases up to $x = 0.75$ in $YMn_{1-x}(Cu_{3/4}Mo_{1/4})_xO_3$. This indicates that the $Mn^{3+}$–O–$Mn^{3+}$ antiferromagnetic interactions are weakened as the Mn array is diluted by the $(Cu_{3/4}Mo_{1/4})^{3+}$ less magnetic cation. However, for the fully substituted ($x = 1$) member, $YCu_{3/4}Mo_{1/4}O_3$, $|\theta_p|$ is higher, $\theta_p = -294$ K which is consistent with the very large absolute value deduced for $LaCu_{3/4}Mo_{1/4}O_3$, $\theta_p = -460$ K. This is to be related to the strength of the $Cu^{2+}$–O–$Cu^{2+}$ antiferromagnetic fluctuations, which dominates in $YCu_{3/4}Mo_{1/4}O_3$.

Table 4
Paramagnetic temperature $\theta_p$ effective paramagnetic moment $\mu_{eff}$ (experimental "exp" and theoretical "th") of compounds $YMn_{1-x}(Cu_{3/4}Mo_{1/4})_xO_3$

| $x$ | $\theta_p$ (K) | $\mu^2_{eff}$ (exp) ($\mu_B$/mol) | $\mu^2_{eff}$ (th) ($\mu_B$/mol) |
|---|---|---|---|
| 0 | −490 | 28 | 24 |
| 0.25 | −300 | 17.3 | 18.7 |
| 0.5 | −201 | 11 | 13.1 |
| 0.75 | −156 | 5.9 | 7.7 |
| 1 | −294 | 1.8 | 2.2 |

The values are extracted by a Curie–Weiss law fitting of the $\chi^{-1}(T)$ for $T$ in the range 250 to 400 K.

As a consequence of this $|\theta_p|$ decrease as $x$ increases, the Néel temperature, $T_N$, of $YMnO_3$, which is indicated by an arrow in the insert of Fig. 7 ($T_N \sim 75$ K), decreases rapidly down to $T_N \sim 30$ K for $x = 0.25$. For the other compositions, $x = 0.5$ and $x = 0.75$, the $\chi^{-1}(T)$ shape is different with a progressive rounding developing below $\sim 200$ K and without a bump as in $YMnO_3$. This suggests a lack of long-range magnetic ordering, even for the lowest temperature, for both $x = 0.5$ and $x = 0.75$ compounds. This is a direct consequence of the magnetic disordering induced by the presence of the random distribution of three different cations on the B-site.

Finally, the shape of the $\chi^{-1}(T)$ curve of the end member, $YCu_{3/4}Mo_{1/4}O_3$, differs from that of the $x = 0.5$ and $x = 0.75$

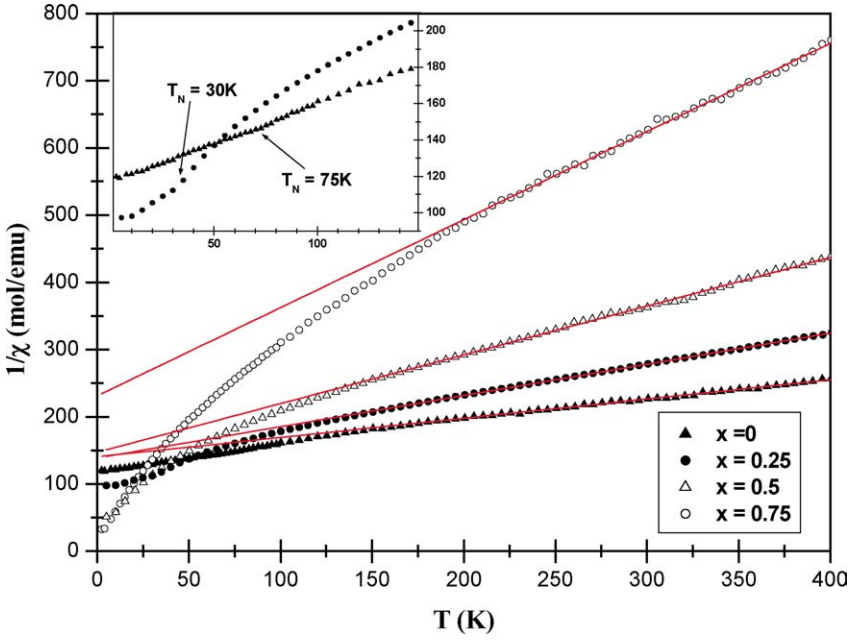


Fig. 7. Temperature ($T$) dependence of the inverse magnetic susceptibility ($\chi^{-1}$) for representative samples of the $YMn_{1-x}(Cu_{3/4}Mo_{1/4})_xO_3$ series. The $x$ values are labeled in the graph. The straight lines are for the fitting curves obtained by using the Curie–Weiss law (see text). The arrows for the $x = 0$ and $x = 0.25$ compounds are for $T_N$.

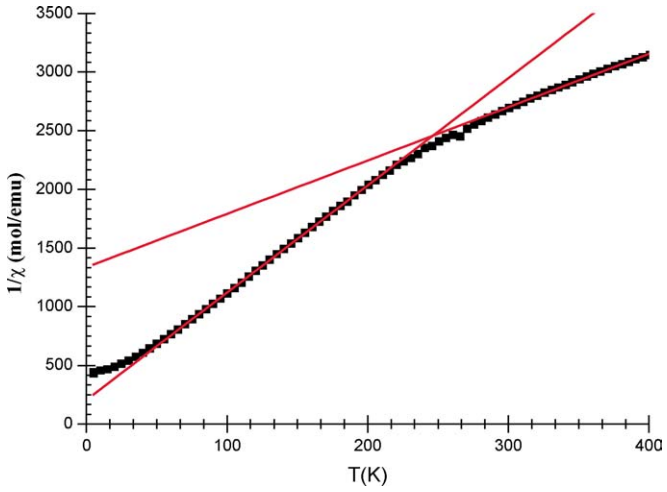


Fig. 8. $\chi^{-1}(T)$ curve for $YCu_{3/4}Mo_{1/4}O_3$. The two straight lines are the two Curie–Weiss fitting.

compounds (Fig. 8). For thus compounds, the metallic cations $Cu^{2+}$ and $Mo^{6+}$ are ordered on a triangular network. Taking into account the triangular frustration induced by the corner shared trigonal bipyramids, one would expect a lack of magnetic ordering as it was already reported for $La_4Cu_3MoO_{12}$ [16] and $La_3Cu_2VO_9$ [15]. Consequently, the magnetic state has been assumed to be also paramagnetic for $YCu_{3/4}Mo_{1/4}O_3$. Two linear $\chi^{-1}(T)$ regimes can be distinguished: one at high temperature, which has already been discussed with all the $Cu^{2+}$ ($S = 1/2$) magnetic moments contributing to the paramagnetism, and, a second regime, at lower temperature, leading to $\mu_{\text{eff}} = 0.95\mu_B/\text{Cu}$. From this experimental value, one obtains that only 30% of the Cu magnetic moments are detected. For this compound, the $T$ dependent magnetic behavior is just as if the $Cu^{2+}$ cations are loosing 2/3 of their magnetic moment as $T$ decreases (at high temperature, $\mu_{\text{eff}} = 1.8\mu_B/\text{Cu}$ instead of $\mu_{\text{eff}} = 1.73\mu_B/\text{Cu}$ but at low $T$, $\mu_{\text{eff}} = 0.95\mu_B/\text{Cu}$). This is reminiscent of a triangular frustration: if three $Cu^{2+}$ cations occupy the corners of the same triangle, two cations over three can be antiferromagnetically paired yielding no net magnetic contribution and only the third $Cu^{2+}$ contributes. Such a situation neglects the presence of the $d^0$ $Mo^{6+}$ cations which would release the frustration when occupying the corner of the triangle instead of copper. The only possibility would be thus that the $Cu^{2+}$ form always triplet and that $Mo^{6+}$ cations order in between these triangles. Such a magnetic distribution was found in the case of $La_4Cu_3MoO_{12}$ which exhibits a supercell derived from the $YMnO_3$ structure.

## 5. Discussion and concluding remarks

The present study of the structural and magnetic properties for the complex $YMn_{1-x}(Cu_{3/4}Mo_{1/4})_xO_3$ system demonstrates that a disordered solid solution can be obtained for $0 \leqslant x < 0.9$, the hexagonal structure of the limit member $YMnO_3$ being preserved. This is an important result with regard to previous studies of different $YMn_{1-x}M_xO_3$ series ($M$ = transition metal) which evidenced a phase transition from the hexagonal structure to the orthorhombic perovskite structure, for instance, as soon as $x \sim 0.15$ for Co. Note that the orthorhombic perovskite form can be also stabilized working under high pressure or in the form of thin films [19,20]. This shows that the role of transition or post transition metal is important and deserves to be investigated. The limit $x = 1$ member, $YCu_{3/4}Mo_{1/4}O_3$, exhibits a complex monoclinic and original superstructure different from the one reported for $LaCu_{3/4}Mo_{1/4}O_3$ [16]. Thus, the electron diffraction study evidence the presence of the two types structures, disordered and ordered, depending on the $x$ value in $YMn_{1-x}(Cu_{3/4}Mo_{1/4})_xO_3$. The accurate determination of the cations ordering mechanisms for $x = 1$, using X-ray diffraction and high-resolution electron microscopy is in progress.

For all the "disordered" compounds ($x < 0.9$) it must be pointed out that the non-centrosymmetry ($P6_3cm$ space group) is preserved. This could allow ferroelectricity to exist. Nonetheless, according to the magnetic dilution of the manganese network induced by the ($Cu^{2+}/Mo^{6+}$) cations one could speculate that the interplay between the charges and spins decreases as $x$ increases in $YMn_{1-x}(Cu_{3/4}Mo_{1/4})_xO_3$. Dielectric measurements as a function of $T$ are now under progress to test this hypothesis.

## References

[1] W. Prellier, A. Fouchet, B. Mercey, J. Phys. Condens. Matter 15 (2003) R1583.
[2] H.L. Yakel, W.C. Koehler, E.F. Bertaut, E.F. Forrat, Acta Cryst. 16 (1963) 957.
[3] G.A. Smolenskii, V.A. Bokov, J. Appl. Phys. 35 (1964) 915.
[4] E.F. Bertaut, R. Pauthenet, M. Mercier, Phys. Lett. 7 (1963) 110; E.F. Bertaut, R. Pauthenet, M. Mercier, Phys. Lett. 18 (1965) 13.
[5] Z.J. Huang, Y. Cao, Y.Y. Sun, Y.Y. Xue, C.W. Chu, Phys. Rev. B 56 (1997) 2623.
[6] O. Muller, R. Roy, in: The Major Ternary Structural Families, Springer-Verlag, New York, 1974, pp. 357–358.
[7] B.B. van Aken, A. Meetsma, T.M. Palstra, Acta Cryst. C 57 (2001) 230.
[8] A. Filippeti, N.A. Hill, Phys. Rev. B 65 (2002) 195120.
[9] C. Moure, D. Gutierrez, O. Peña, P. Duran, J. Solid State Chem. 163 (2002) 377.
[10] D.A. Vander Griend, S. Boudin, K.R. Poeppelmeier, M. Azuma, H. Toganoh, M. Takano, J. Am. Chem. Soc. 120 (1998) 11518.
[11] H. Ismailzade, G.A. Smolenskii, V.I. Nesterenko, F.A. Agaev, Phys. Stat. Sol. A 5 (1971) 83.
[12] D.A. Vander Griend, S. Malo, K.T. Wang, K.R. Poeppelmeier, J. Am. Chem. Soc. 122 (2000) 7308.
[13] N. Floros, J.T. Rijssenbeek, A.B. Martinson, K.R. Poeppelmeier, Solid State Sci. 4 (2002) 1495.
[14] K. Jansson, I. Bryntse, Y. Teraoka, Mater. Res. Bull. 31 (1996) 827.
[15] D.A. Vander Griend, S. Malo, S.J. Bary, N.M. Dabbousch, K.R. Poeppelmeier, V.P. Dravid, Solid State Sci. 3 (2001) 569.
[16] D.A. Vander Griend, S. Boudin, V. Caignaert, K.R. Poeppelmeier, Y. Wang, V.P. Dravid, M. Azuma, M. Takano, Z. Hu, J.D. Jorgensen, J. Am. Chem. Soc. 121 (1999) 4787.
[17] M. Azuma, T. Odaka, M. Takano, D.A. Vander Griend, K.R. Poeppelmeier, Y. Narumi, K. Kindo, Y. Mizuno, S. Maekawa, Phys. Rev. B 62 (2000) R3588.
[18] E.F. Bertaut, J. Mareschal, Comptes Rendus 275 (1963) 867.
[19] H.W. Brinks, H. Fjellvag, A. Kjekshus, J. Solid State Chem. 129 (1997) 334.
[20] A. Waintal, J. Chevanas, Mater. Res. Bull. 2 (1967) 819.
[21] D.M. Giaquinta, H.C. Zur Loye, J. Am. Chem. Soc. 114 (1992) 10952.